

IMECE2005-80459

COMPUTATION OF MULTIPHASE FLOWS WITH LATTICE BOLTZMANN METHODS

Kannan N. Premnath
MetaHeuristics LLC
Santa Barbara, CA 93105
Email: nandha@metah.com

Jean-Christophe Nave
MetaHeuristics LLC
Santa Barbara, CA 93106
Email: jcnave@metah.com

Sanjoy Banerjee
Department of Chemical Engineering
University of California, Santa Barbara
Santa Barbara, CA 93106
Email: banerjee@engineering.ucsb.edu

ABSTRACT

Lattice Boltzmann methods (LBM) have several features that make them attractive for computation of large fluid mechanics problems in complex geometries. For example, in comparison with the conventional projection methods that are widely used in computational fluid dynamics, LBM does not require solution of a pressure Poisson equation which usually accounts for ~ 80% of the computational time required per time step, and it is also local, making parallelization straightforward, and run time on distributed memory architectures linearly scalable. LBM has therefore been considered for direct simulation of multiphase flows, but its application has been limited because of instabilities that arise when the viscosities become small and/or the density mismatch between the fluids is large. Current approaches to computation of multiphase systems using LBM are reviewed, and new approaches based on multiple relaxation times and a regularization procedure which maintain stability at low viscosities are discussed and a technique using time-splitting, that alleviates the density ratio constraint, is proposed. Applications of the LBM to magnetohydrodynamic (MHD) multiphase flows will be discussed.

INTRODUCTION

Multiphase flows are ubiquitous in nature and in many engineering applications. Direct numerical simulations of such flows require determination of interfacial locations and shapes in conjunction with the flow field and are extremely challenging. Multiple length and time scales also arise and add to the difficulty. Conventionally, methods such as front-

tracking [1], volume-of-fluid [2], level set [3] or phase-field [4] are employed. They involve a direct solution of the continuum equations, including an auxiliary equation for interface motion and the usual conservation equations for mass and momentum. These are generally solved by the projection method [5, 6].

The lattice Boltzmann method (LBM) is a relatively new computational approach for fluid dynamics [7, 8]. It is based on kinetic theory. It involves the solution of the so-called lattice Boltzmann equation (LBE), which is a simplified form of the Boltzmann equation [9]. This equation describes the evolution of the distribution of populations of particles at scales smaller than macroscopic scales and greater than molecular scales. The distribution of the particle populations is modified by the advection and collisions of the particles which occur on a lattice. The lattice, respecting sufficient translational and rotational symmetries, restricts the movement and interactions of particles to a relatively small set of discrete directions such that in the continuum, the collective behavior of the particle populations corresponds to the dynamics of fluid flow described by the weakly compressible Navier-Stokes equations. Since the boundary conditions can be handled with relative ease, the LBM is suitable for handling complex geometries. Moreover, the pressure field is calculated locally from the distribution function thereby avoiding the time-consuming solution of Poisson-type equation involved in the projection method. Since the procedure involves operations that are local and explicit, they are naturally suitable for implementation on parallel computers.

From a physical point of view, since the LBM computes the evolution of the distribution function at scales smaller than the macroscopic scale, physical models for complex fluids that are derived from kinetic theory can be naturally incorporated. The rapid development of the LBM has been documented in several review papers [7, 10-14] and monographs [8, 15].

REVIEW OF MULTIPHASE FLOW MODELS

In the case of multiphase flows, the earliest LBMs were somewhat ad hoc in nature. In essence, two different particle populations, identified by different colors, were used to distinguish the phases. Phase separation was maintained by a recoloring step which forced the particle populations representing colored fluids to move towards fluids with the same color [16, 17]. Subsequent models were developed with a greater physical basis. In these models, phase segregation and interfacial dynamics could be simulated with mean-field forces based on inter-particle potentials [18-20] or by concepts derived from a free energy functional [21, 22]. It was shown out that the LBM based on the latter ideas has certain unphysical features, such as the lack of Galilean invariance [23]. This limitation was alleviated in [24].

The LBM multiphase flow models have been evaluated and compared with analytical or other numerical methods or experimental data for standard benchmark problems in 3D such as drop oscillations, drop deformation and breakup in shear flow, dynamics of rising bubbles and Rayleigh-Taylor instability, all of which show good agreement [25-28]. For high resolution computations required to resolve finer multiphase flow structures, an axisymmetric LBM multiphase flow model that introduces curvature effects to a 2D model has been developed and evaluated for various canonical problems including Rayleigh instability, including the generation of drops from cylindrical liquid columns [29]. While these studies have been promising, LBM multiphase flow models have certain limitations that need to be overcome so that it becomes a more reliable approach for practical applications.

One limitation is that the standard LBM employs a Bhatnagar-Gross-Krook (BGK) model [30] to represent the effect of collision on the distribution of particle populations. According to this model, collisions cause the distribution functions to approach their local equilibrium values at a rate which is determined by a relaxation time parameter. This relaxation time parameter is related to the kinematic viscosity of the fluid being simulated. It has been found that the BGK model becomes unstable as the viscosity becomes smaller or, equivalently, at higher Reynolds numbers. To alleviate this limitation, multiple-relaxation time (MRT) models have been proposed [31-33]. This has recently been extended to multiphase flows [34-37], which were employed to study binary drop collisions [38] and liquid jet break-up [39] and reviewed in detail in [40]. We will discuss such MRT

multiphase models and their application in this paper. Another and more recent approach involves regularizing/renormalizing the non-equilibrium part of the distribution function of the particle populations prior to collisions [41]. This procedure has been generalized for complex fluid flows such as multiphase flows [42] and will be discussed with an application in this paper.

Another important limitation of LBM multiphase flow models is that they are unstable at high density ratios. It is understood that the compressible nature of the method plays an important role in this issue. However, the detailed aspects are still not clearly understood and its solution based on kinetic-theory considerations has not yet been found. Nevertheless, some efforts have been made to address this problem. One of the first attempts involved using a total variation diminishing (TVD) with artificial dissipation scheme [43]. The collision and intermolecular force terms were treated as explicit source terms and time marching is done via a second-order Runge-Kutta scheme. However, this approach severely restricts the range of the relaxation time and Reynolds number. Another approach to alleviate the density ratio limitation employs a projection method has been proposed [44]. This is essentially a heuristic approach and undermines the simplicity and parallelizability of the LBM. Also, an implicit method that uses a set of consistent discretization strategies for the various forcing terms in the LBM for stabilization at higher density ratios has recently been proposed [45].

We have approached this problem from a different perspective. Instead of representing multiphase flow by a single-fluid formulation, that renders the interface diffuse and leads to the interfacial compressibility issues, we solve the flow fields for each phase separately and match the interfacial kinematic and dynamic conditions sequentially, i.e., through time-splitting. The key to this approach is the reconstruction procedure for various interfacial fields based on the interfacial boundary conditions and is obtained by means of a Chapman-Enskog analysis [46]. The interface is advected by means of level sets, while the flow field in each phase is determined by the LBM and various interfacial fields are obtained through a reconstruction procedure that satisfies the velocity and stress boundary conditions in a sequential way. The method circumvents the density ratio problem. Moreover, the computed interfaces are sharp and thus the method has the added potential that computations of high Schmidt/Prandtl number interfacial scalar transfer rates become possible. The basic idea of this method while akin to the ghost-fluid method [47, 48], avoids the solution of the Poisson-type pressure equation. We discuss this approach in this paper.

Physics of free surface/multiphase flows with additional features such as the presence of magnetic fields are important in the proposed liquid wall blanket concepts for fusion

applications [49]. Recently, magnetohydrodynamic (MHD) LBM have been developed for single-phase flows [50, 51]. We have employed these models to simulate MHD multiphase flows and will be discussed in this paper.

The paper is partially a review of previous work such as the MRT model and partially outlines new work related to the regularization procedure, time-splitting model and MHD modeling. It is organized as follows. In the next section, the multiple-relaxation time (MRT) LBM model for multiphase flows will be briefly presented. The reader is referred to [34-37] for details of this model. Then, the regularized model will be discussed. This will be followed by a discussion on the time-splitting approach as applied to LBM for multiphase flow. Then, MHD modeling using LBM will be discussed. Results and discussion follow. The paper concludes with a summary and indicates some directions for future work.

MULTIPLE-RELAXATION TIME (MRT) LATTICE BOLTZMANN MODEL FOR MULTIPHASE FLOWS

The MRT lattice Boltzmann (LB) model [34-37] is based on the solution of the simplified form of the continuous Boltzmann equation for non-ideal fluids given by [19]

$$\frac{\partial f}{\partial t} + \xi \cdot \nabla f = \Omega + \frac{(\xi - \mathbf{u}) \cdot (\mathbf{F} + \mathbf{F}_{ext})}{\rho RT} f^M, \quad (1)$$

where $f \equiv f(\mathbf{x}, \xi, t)$ is the particle distribution function, ξ is the particle velocity, \mathbf{u} is the macroscopic fluid velocity at location \mathbf{x} , Ω represents the change in the distribution function due to collisions, \mathbf{F} represents the mean-field force based on the inter-particle potential between particle populations, and \mathbf{F}_{ext} represents external forces such as gravity and/or Lorentz force in electrically conducting fluids in the presence of magnetic fields. The collision term Ω is commonly modeled by employed the BGK single-relaxation time model [30], according to which $\Omega = -(f - f^M) / \lambda$, where λ is the relaxation time. In this work, on the other hand, the LB model derived from Eq. (1) consists of an MRT collision term.

The equilibrium distribution function, f^M is given by the local Maxwellian

$$f^M = \frac{\rho}{(2\pi RT)^{D/2}} \exp\left[-\frac{(\xi - \mathbf{u})^2}{2RT}\right] \quad (2)$$

where ρ is the density, R is the ideal gas constant, T is the temperature, and D is the dimension of the space. The fluid density and macroscopic momentum are obtained as the zeroth and the first kinetic moments of the distribution function.

The mean-field force \mathbf{F} is modeled as a function of density based on the work of van der Waals [52]. The exclusion-volume effect by Enskog [53] is incorporated to account for the increase in collision probability due to the increase in density of non-ideal fluids. For more details, the reader is referred to [19, 20]. Effectively, this force may be written as

$$\mathbf{F} = -\nabla \psi + \mathbf{F}_s, \quad (3)$$

where the function ψ represents the non-ideal part of the equation of state

$$\psi(\rho) = P - \rho RT. \quad (4)$$

In this model, the Carnahan-Starling-van der Waals equation of state (EOS),

$$P = \rho RT \left[\frac{1 + \theta + \theta^2 - \theta^3}{(1 - \theta)^3} \right] - a\rho^2, \quad (5)$$

is employed where $\theta = b\rho/4$ [54]. The parameter a is related to the inter-particle pair-wise potential and b is related to the effective diameter d of the particle and the mass m of a single particle by $b = 2\pi d^3/3m$.

The function ψ assumes an important role in determining phase segregation [20]. The Carnahan-Starling-van der Waals EOS has a $P - v - T$ curve, in which $dP/d\rho < 0$ for certain range of values of ρ , when the state fluid temperature is below its critical value. This part of the curve represents an unstable physical situation and is the driving mechanism responsible for keeping the phases of fluids segregated and in maintaining a self-generated diffuse interface.

The term \mathbf{F}_s in Eq. (3) represents the surface tension force and is related to the density and its gradient by

$$\mathbf{F}_s = \kappa \rho \nabla \nabla^2 \rho, \quad (6)$$

where κ is a surface tension parameter. This parameter is related to the surface tension σ of the fluid by the equation [55]

$$\sigma = \kappa \int \left(\frac{\partial \rho}{\partial n} \right)^2 dn, \quad (7)$$

where n is the normal direction of the interface. Thus, σ is a function of both the parameter κ and the density profile across the interface. To facilitate the numerical solution of the governing set of equations discussed above, the particle velocity space is discretized with a small discrete set of velocities $\{e_\alpha\}$, where α represents the particle velocity direction. The physical space is discretized such that the discrete distribution function travels from one grid node to its

adjacent node in each time step along the discrete direction α . This coupling of the particle velocity and the physical space comprises the lattice.

The collision term, Ω in the MRT model is modeled as a relaxation process in which the discretized distribution function approaches its local equilibrium value at characteristic time scales given in terms of the components $\Lambda_{\alpha\beta}$ of the collision matrix $\mathbf{\Lambda}$. Thus, the lattice MRT LBE for multiphase flows may be represented by

$$\begin{aligned} \bar{f}_\alpha(\mathbf{x} + \mathbf{e}_\alpha \delta_t, t + \delta_t) - \bar{f}_\alpha(\mathbf{x}, t) \\ = -\Lambda_{\alpha\beta} (\bar{f}_\beta - \bar{f}_\beta^{eq}) + \\ (I_{\alpha\beta} - 1/2\Lambda_{\alpha\beta}) S_\beta \delta_t, \end{aligned} \quad (8)$$

where S_β represents the source term containing the mean-field forces and $I_{\alpha\beta}$ is the component of the identity matrix \mathbf{I} .

When the distribution functions are multiplied by an appropriate transformation matrix \mathbf{T} (see [32, 34] for two-dimensional problems and [33, 36] for three-dimensional problems), they can be mapped to a moment space. In the moment space, the collision matrix $\mathbf{\Lambda}$ becomes a diagonal matrix. The moments fall into the categories of conserved moments, such as density and momentum, and non-conserved moments, such as viscous stress and kinetic moments. Physically, collisions do not change the conserved moments while the non-conserved moments relax to their equilibrium values which are algebraic functions of the conserved moments [32, 33]. For multiphase phase flows, these moments are related to phase segregation terms and surface tension through a Chapman-Enskog analysis [34, 36]. Since some of the moments of the distribution functions, such as the components of the viscous stress, carry direct physical import, the relaxation parameters in the resulting diagonal collision matrix are directly related to the various transport coefficients, such as bulk and shear viscosities. This allows independent control of the time scales of the various hydrodynamic modes and thus improves stability, particularly at lower shear viscosities, where the standard LBM models are prone to instability. Next, we discuss an alternative technique, i.e. the regularization procedure to improve stability.

REGULARIZED LATTICE BOLTZMANN MODEL FOR MULTIPHASE FLOWS

In regularized LBM, instead of using a MRT matrix, the standard BGK collision term is retained. However, the distribution functions prior to collisions are renormalized. This has been shown to result in significant improvement in stability for single-phase flows [41]. Here, we present its generalization to multiphase flows. In the following, we consider Greek symbols for particle velocity directions and Latin symbols for Cartesian components of spatial directions

and assume summation convention for repeated indices of Cartesian components. The starting point is the LBE with a force interaction term, which can be algorithmically split into the collision step with forcing term update

$$\tilde{f}_\alpha(\mathbf{x}, t) = \bar{f}_\alpha(\mathbf{x}, t) + \bar{\Omega}_\alpha + \left(1 - \frac{1}{2\tau}\right) S_\alpha|_{(\mathbf{x}, t)} \delta_t, \quad (9)$$

where \tilde{f}_α represents the post-collision distribution function and the streaming step

$$\bar{f}_\alpha(\mathbf{x} + \mathbf{e}_\alpha \delta_t, t + \delta_t) = \tilde{f}_\alpha(\mathbf{x}, t). \quad (10)$$

Here, \mathbf{e}_α represents the lattice velocity direction. In the collision step, \bar{f}_α to relax to its equilibrium value f_α^{eq} in a characteristic time $\tau\delta_t$, where δ_t is the time step, i.e. the collision term $\bar{\Omega}_\alpha$ becomes

$$\bar{\Omega}_\alpha = -\frac{1}{\tau} (\bar{f}_\alpha - f_\alpha^{eq}) \quad (11)$$

and further modified by the presence of forces through S_α . The streaming step represents the change in \bar{f}_α as the particles stream along their characteristics \mathbf{e}_α , with a speed c , where $c = \delta_x / \delta_t$, from one lattice node to its adjacent one, which are separated a distance whose Cartesian component is δ_x . The equilibrium distribution function f_α^{eq} in Eq. (11) is given by

$$f_\alpha^{eq} = w_\alpha \rho \left\{ 1 + \frac{e_{\alpha k}}{c_s^2} u_k + \frac{Q_{\alpha ij}}{2c_s^4} u_i u_j \right\}, \quad (12)$$

with

$$Q_{\alpha ij} = e_{\alpha i} e_{\alpha j} - c_s^2 \delta_{ij} \quad (13)$$

being the second-order, symmetric lattice velocity tensor. Here, δ_{ij} is the Kronecker delta, w_α is the weighting factor [7] and

$$c_s = 1/\sqrt{3} c \quad (14)$$

is the speed of sound. The source term S_α representing the effect of force interactions may be written as

$$S_\alpha = \frac{(\mathbf{e}_\alpha - \mathbf{u}) \cdot (\mathbf{F} + \mathbf{F}_{ext})}{\rho c_s^2} f_\alpha^{eq}, \quad (15)$$

where \mathbf{F} is the mean-field force given in Eq. (3) and \mathbf{F}_{ext} represents forces such as gravity and/or Lorentz force.

The key element in the regularization procedure is to expand the distribution function \bar{f}_α around its local equilibrium value

$$\bar{f}_\alpha = \bar{f}_\alpha^* \equiv f_\alpha^{eq} + \delta_t f_\alpha^{(1)}, \quad (16)$$

and substitute in the collision step, i.e. Eq. (9), so that it regularizes to the following:

$$\tilde{\bar{f}}_\alpha(\mathbf{x}, t) = f_\alpha^{eq} + \left(1 - \frac{1}{\tau}\right) \bar{f}_\alpha^{(1)} \delta_t + \left(1 - \frac{1}{2\tau}\right) S_\alpha \delta_t. \quad (17)$$

Applying Chapman-Enskog analysis [53] yields the non-equilibrium part of the distribution function $f_\alpha^{(1)}$ as [42]

$$\begin{aligned} \bar{f}_\alpha^{(1)} = & \frac{w_\alpha}{2c_s^4} \bar{\Pi}_{ij}^{(1)} Q_{\alpha ij} + \frac{w_\alpha}{2c_s^4} \left((F_i + F_{ext,i}) u_j \right) Q_{\alpha ij} \\ & - \frac{\tau w_\alpha}{c_s^2} e_{\alpha k} (F_k + F_{ext,k}) + \left(\tau - \frac{1}{2} \right) S_\alpha \\ & - \frac{\tau w_\alpha}{c_s^2} (u_i \partial_j \rho) Q_{\alpha ij}, \end{aligned} \quad (18)$$

where $\bar{\Pi}_{ij}^{(1)}$ is the non-equilibrium momentum flux tensor given by

$$\bar{\Pi}_{ij}^{(1)} = \sum_\alpha e_{\alpha i} e_{\alpha j} (\bar{f}_\alpha - f_\alpha^{eq}). \quad (19)$$

Eq. (18) is the main result of this section. The first term on the right hand side (RHS) of this equation corresponds to that given in [41], while second, third and fourth terms arise due to force interactions and the last term occurs when there are spatial gradients in density, such as that across interfaces in multiphase flows [42]. The density ρ and the velocity fields \mathbf{u} can be obtained from the distribution function as

$$\rho = \sum_\alpha \bar{f}_\alpha, \quad (20)$$

$$\rho \mathbf{u} = \sum_\alpha \bar{f}_\alpha \mathbf{e}_\alpha + \frac{1}{2} (\mathbf{F} + \mathbf{F}_{ext}) \delta_t, \quad (21)$$

$$\nu = c_s^2 \left(\tau - \frac{1}{2} \right) \delta_t. \quad (22)$$

Equations (10)-(15) and (17)-(22) constitute the regularized LBM with force fields such as that for multiphase flows.

The reason for improvement in stability of this model becomes apparent when it is considered in the moment space as was done with the MRT model in the previous section. This is done by multiplying Eq. (18) by the transformation matrix \mathbf{T} [32, 33]. The collision matrix effectively becomes

$$\hat{\mathbf{A}}^* = (1 - 1/\tau) \mathbf{T} \mathbf{R} \mathbf{T}^{-1} \text{ where the components of } \mathbf{R} \text{ are } R_{\alpha\beta} = \frac{w_\alpha}{2c_s^4} Q_{\alpha ij} e_{\beta i} e_{\beta j}. \hat{\mathbf{A}}^* \text{ has contributions to}$$

hydrodynamic moments or physical modes only and but not to kinetic moments, sometimes also called ghost or spurious modes, which exist for the standard BGK model. That is, the regularization procedure radically eliminates all the non-

physical modes. In the case of single phase flows, compared to the standard BGK model, the regularized model has been shown to be more accurate apart from significantly improved stability [41]. While the MRT model is more general, the regularized model is simpler and more efficient to implement. It may be noted that in moment space, the forcing term components in Eq. (19), i.e. the second and third terms on the RHS have mutually orthogonal contributions, while the rest have full contributions [42]. In the Results and Discussion section, we will discuss an application of this procedure to multiphase flows. Next, we discuss the proposed time-splitting LBM for interfacial multiphase flows.

TIME-SPLIT LATTICE BOLTZMANN MODEL FOR MULTIPHASE FLOWS

Consider a two-phase system, consisting of the liquid phase with ρ_L and ν_L as density and kinematic viscosity, respectively, and the gas phase with ρ_G and ν_G as density and kinematic viscosity, respectively, as shown in Fig. 1. At time t , the liquid and gas phases occupy locations $\mathbf{x} \in \{\mathbf{x}_L\}$ and $\mathbf{x} \in \{\mathbf{x}_G\}$, respectively, and are separated by a sharp interface \mathcal{S} . For generality, it is assumed that the fluids are subjected to external force field $\mathbf{F} = \rho \mathbf{a}$, where \mathbf{a} is the acceleration, such as gravity. The domain is considered to be discretized by means of a two-dimensional, nine-velocity (D2Q9) lattice model. The flow field in each phase can be represented by the averaged effect of the distribution function \bar{f}_α , where α is one of the nine velocity directions, whose evolution is given by the lattice Boltzmann equation (LBE)

$$\begin{aligned} \bar{f}_\alpha(\mathbf{x} + \mathbf{e}_\alpha \delta_t, t + \delta_t) - \bar{f}_\alpha(\mathbf{x}, t) = \\ - \frac{1}{\tau} (\bar{f}_\alpha - f_\alpha^{eq}) \Big|_{(\mathbf{x}, t)} + \left(1 - \frac{1}{2\tau}\right) S_\alpha \Big|_{(\mathbf{x}, t)} \delta_t \end{aligned} \quad (23)$$

which is essentially the combined form of Eqs. (9) and (10).

The equilibrium distribution is given by

$$f_\alpha^{eq} = w_\alpha \left\{ \rho + \frac{e_{\alpha k}}{c_s^2} j_k + \frac{e_{\alpha i} e_{\alpha j}}{2c_s^4} \frac{j_i j_k}{\rho} - \frac{1}{2c_s^2} \frac{j_k j_k}{\rho} \right\}, \quad (24)$$

where the subscripts $i, j, k \in \{x, y\}$ and as before the summation convention of repeated indices is assumed. Here j_i is the Cartesian component in the i -direction of momentum $\mathbf{j} \equiv \rho \mathbf{u}$, where \mathbf{u} is the velocity. The weighting factor w_α is given by

$$w_\alpha = \begin{cases} 4/9 & \alpha = 0 \\ 1/9 & \alpha = 1, 2, 3, 4 \\ 1/36 & \alpha = 5, 6, 7, 8 \end{cases} \quad (25)$$

The source term S_α for the external force field in Eq. (23) is the same as Eq. (15), with $\mathbf{F} + \mathbf{F}_{ext}$ replaced by $\rho\mathbf{a}$. The macroscopic fields, such as density and momentum in each phase are obtained by taking kinetic moments and the pressure, are obtained directly from density:

$$\rho = \sum_\alpha \bar{f}_\alpha, \quad (26)$$

$$\mathbf{j} = \sum_\alpha \bar{f}_\alpha \mathbf{e}_\alpha + \frac{1}{2} (\rho\mathbf{a}) \delta_t, \quad (27)$$

$$P = \rho c_s^2. \quad (28)$$

As in the previous section, the above macroscopic fields satisfy the weakly compressible Navier-Stokes equations in the continuum limit, whose kinematic viscosity is related to the lattice parameters as given in Eq. (22).

At the interface S , where a local coordinate system $\{\mathbf{n}, \mathbf{T}\}$ is set up, wherein \mathbf{n} and \mathbf{T} are the local normal and tangent, respectively (see Fig. 1), interfacial physics through jump conditions needs to be satisfied by the macroscopic fields. They are given by

$$\frac{j_{xG}}{\rho_G} - \frac{j_{xL}}{\rho_L} = 0, \quad (29)$$

$$\frac{j_{yG}}{\rho_G} - \frac{j_{yL}}{\rho_L} = 0, \quad (30)$$

$$(-P + 2\nu\partial_n j_n)_G - (-P + 2\nu\partial_n j_n)_L = \sigma\mathcal{K}_{curv}, \quad (31)$$

$$(\nu(\partial_n j_T + \partial_T j_n))_G - (\nu(\partial_n j_T + \partial_T j_n))_L = 0. \quad (32)$$

Equations (29) and (30) are the kinematic conditions of the continuity of the velocity fields, while Eqs. (31) and (32) are the dynamic conditions based on stresses. Here, σ and \mathcal{K}_{curv} are surface tension and local curvature, respectively. Since the LBM solves the distribution functions, i.e. mesoscopic variables, while the interfacial conditions are given in terms of macroscopic field variables, the main feature of the proposed approach is the development of a procedure that incorporates the latter in the former in a physically consistent way.

As in the previous section, the starting point for the procedure involves expanding the distribution function around its local equilibrium,

$$\bar{f}_\alpha = f_\alpha^{eq} + \delta_t \bar{f}_\alpha^{(1)} + \dots, \quad (33)$$

where the non-equilibrium part $\bar{f}_\alpha^{(1)}$ can be written in terms of momentum gradient tensor $\partial_j j_i$ and external acceleration \mathbf{a}_k through the Chapman-Enskog analysis [53]

$$\bar{f}_\alpha^{(1)} = -\frac{\tau w_\alpha}{c_s^2} (\partial_j j_i) Q_{\alpha ij} - \frac{\tau w_\alpha}{c_s^2} (e_{\alpha k} a_k) \rho + \left(\tau - \frac{1}{2} \right) S_\alpha, \quad (34)$$

where $Q_{\alpha ij}$ is given in Eq. (13). Following [56, 57], since Eq. (34) is rotationally invariant with respect to any orthogonal coordinate system, Eqs. (33) & (34) can be written in terms of the local interface coordinate system $\{\mathbf{n}, \mathbf{T}\}$ and by assuming incompressibility condition and neglecting terms that are higher order in Mach number, i.e. $O(Ma^2)$ or higher and linearizing the nonlinear terms and after some simplification, we get for $\alpha = 0, 1, \dots, 8$ [46]

$$\bar{f}_\alpha = w_\alpha \left\{ C_r' \rho + C_{m1}' j_x + C_{m2}' j_y \right\} - \frac{\tau \delta_t}{c_s^2} w_\alpha \left\{ C_{shs} (\partial_n j_T + \partial_T j_n) + C_{nors} \partial_n j_n \right\}, \quad (35)$$

where the coefficients are given by

$$C_r' = 1 - \tau \delta_t \frac{(e_{\alpha k} a_k)}{c_s^2} + \left(\tau - \frac{1}{2} \right) \delta_t E_{c\alpha}^* (e_{\alpha k} a_k),$$

$$C_{m1}' = E_{d\alpha}^* e_{\alpha x} - \frac{u_x^*}{2c_s^2} - \left(\tau - \frac{1}{2} \right) \delta_t E_{c\alpha}^* a_x,$$

$$C_{m2}' = E_{d\alpha}^* e_{\alpha y} - \frac{u_y^*}{2c_s^2} - \left(\tau - \frac{1}{2} \right) \delta_t E_{c\alpha}^* a_y,$$

$$C_{shs} = Q_{\alpha n T} = e_{\alpha n} e_{\alpha T},$$

$$C_{nors} = 2Q_{\alpha n n} - ((e_{\alpha n}^2 + e_{\alpha T}^2) - 2c_s^2) = e_{\alpha n}^2 - e_{\alpha T}^2.$$

Here,

$$E_{c\alpha}^* = \left[\frac{1}{c_s^2} + \frac{E_\alpha^*}{c_s^4} \right], \quad E_{d\alpha}^* = \left[\frac{1}{c_s^2} + \frac{E_\alpha^*}{2c_s^4} \right], \quad E_\alpha^* = e_{\alpha k} u_k^*,$$

$$e_{\alpha n} = \mathbf{e}_\alpha \cdot \mathbf{n}, \quad e_{\alpha T} = \mathbf{e}_\alpha \cdot \mathbf{T},$$

where \mathbf{u}^* is appropriately spatially or temporally extrapolated value of velocity at a given node and \mathbf{n} and \mathbf{T} are local normal and tangent, respectively. Equation (35) is the key equation in the procedure. Notice that according to this equation, the distribution function is a function of density (or pressure), components of momentum and interfacial momentum gradient tensor.

Depending on the interface topology, the distribution functions corresponding to certain directions that arrive from the other side of a given phase are unknown. As an illustration,

in Fig. 1 at location \mathbf{x} , the distribution functions corresponding to directions $\alpha = 1, 4, 7, 8$ are unknown on the liquid side, while those for $\alpha = 2, 3, 5, 6$ are unknown on the gas side. So, in general, let $\alpha \in V^-$ and $\alpha \in V^+$ represent the set of unknown and known directions, respectively, for a given phase, with $n(V^-)$ and $n(V^+)$ being the corresponding number of unknown and known directions, respectively. Obviously, $n(V^+ \cup V^-) = 9$. Now, the interfacial jump conditions, Eqs. (29) - (32), need to be satisfied in computing the unknowns. To this end, we follow a time-splitting procedure, where in a given time step the stress boundary conditions from the gas side is employed to determine the unknown distribution functions and interfacial momentum and density (or pressure) and followed by applying the velocity (or momentum) boundary conditions from the liquid side to determine the unknown distribution functions and interfacial momentum gradient tensor and density (or pressure).

Hence, for the interfacial nodes on the *liquid side*, using Eqs. (31) and (32) in Eq. (35), we get for $\alpha = 0, 1, \dots, 8$

$$\bar{f}_\alpha = w_\alpha \left\{ C'_r \rho_L + C'_{m1} j_{xL} + C'_{m2} j_{yL} \right\} - \frac{\tau \delta_t}{c_s^2} w_\alpha \left\{ C_{shs} \left[\frac{v_G}{v_L} (\partial_n j_T + \partial_T j_n)_G \right] + C_{nors} \left[\frac{(P_L - P_G) - \sigma \kappa_{curv}}{2v_L} + \frac{v_G}{v_L} (\partial_n j_n)_G \right] \right\} \quad (36)$$

Here, the unknowns are \bar{f}_α for $\alpha \in V^-$ and j_{xL}, j_{yL} and ρ_L or P_L . And, for the interfacial nodes on the *gas side*, using Eqs. (29) and (30) in Eq. (35), we get for $\alpha = 0, 1, \dots, 8$

$$\bar{f}_\alpha = w_\alpha \left\{ C'_r \rho_G + C'_{m1} \left(\frac{j_{xL}}{\rho_L} \right) \rho_G + C'_{m2} \left(\frac{j_{yL}}{\rho_L} \right) \rho_G \right\} - \frac{\tau \delta_t}{c_s^2} w_\alpha \left\{ C_{shs} (\partial_n j_T + \partial_T j_n)_G + C_{nors} (\partial_n j_n)_G \right\} \quad (37)$$

Here, the unknowns are \bar{f}_α for $\alpha \in V^-$ and $(\partial_n j_T + \partial_T j_n)_G, (\partial_n j_n)_G, \rho_G$ or P_G . In Eqs. (36) and (37), the relaxation time τ is chosen such that it is used to determine the respective kinematic viscosity of each phase using Eq. (22).

Notice that on each side, the total number of unknown interfacial fields, which are a $n(V^-)$ set of mesoscopic and 3 macroscopic or hydrodynamic fields, $n(V^-) + 3$ changes depending on the shape of the interface. On each side, the total number of equations available to determine the

unknowns, which are $n(V^+)$ set of equations for $\alpha \in V^+$ and a mass conservation constraint $\sum_{\alpha \in V^-} \bar{f}_\alpha + \sum_{\alpha \in V^+} \bar{f}_\alpha = \rho$

providing $n(V^+) + 1$ equations. Thus, the number of unknown fields can be different from the number of equations available to solve them. Generally, the number of equations exceeds the number of unknowns. As a result, a *least squares method* is employed to determine the unknown fields. In essence, on each side, first the 3 unknown macroscopic fields are solved by using $n(V^+) + 1$ equations that corresponds to Eq. (36) or (37), as appropriate, for $\alpha \in V^-$ and the mass conservation constraint through a least squares approach. Once, the macroscopic fields are known, Eq. (36) or (37) can be employed to determine the $n(V^-)$ unknown mesoscopic fields through a simple substitution. With the velocity fields known, the interface is advected by a kinematic equation for the level set function ϕ

$$\partial_t \phi + \mathbf{u} \cdot \nabla \phi = 0. \quad (38)$$

$\phi > 0$ represents liquid phase, while $\phi < 0$ corresponds to gas phase and $\phi = 0$ the interface. To maintain ϕ as the signed distance function, it is *reinitialized* using a suitable partial differential equation without changing its zero level set [3]. Once the level set function is known, interface topological information such as normals \mathbf{n} , tangents \mathbf{T} and curvature κ_{curv} can be computed.

Hence, in summary, the time-splitting LB approach for multiphase flows involves the following sub-computational steps for each time step:

- (i) Interface is advected by using a *level set method*, which also provides the normals, tangents and curvatures at the interface. (*Interface Advection Step*)
- (ii) For lattice nodes closer to the interface on the *gas side*, (a) First, $(\partial_n j_T + \partial_T j_n)_G, (\partial_n j_n)_G$ and ρ_G or P_G is computed from Eq. (26) for $\alpha \in V^+$ and a mass conservation constraint through a *least squares method*. (b) Next, \bar{f}_α for $\alpha \in V^-$ is obtained from Eq. (26) through substitution. (*Gas Interfacial Reconstruction Step*)
- (iii) For lattice nodes closer to the interface on the *liquid side*, (a) First, j_{xL}, j_{yL} and ρ_L or P_L is computed from Eq. (25) for $\alpha \in V^+$ and a mass conservation constraint through a *least squares method*. (b) Next, \bar{f}_α for $\alpha \in V^-$ is obtained from

Eq. (25) through substitution. (*Liquid Interfacial Reconstruction Step*)

- (iv) On *each* side, for lattice nodes away from the interface, from Eqs. (10), i.e. the *LBE*, through (16) the distribution functions and the flow field (ρ , \mathbf{u} and P) can be computed. (*Bulk Flow field Computational Step*)

While we have restricted our discussion on this approach to 2D for reasons of brevity, it can be readily extended to 3D [46]. Notice that this procedure avoids the solution of a Poisson-type equation for pressure. Next, we briefly discuss the MHD flow modeling using LBM.

MAGNETOHYDRODYNAMIC (MHD) FLOW MODELING USING LATTICE BOLTZMANN METHOD

In electrically conducting fluid flows in the presence of magnetic field \mathbf{B} , a body force – the Lorentz force – is generated due to the interactions between the flow field, magnetic field and the induced current. The Lorentz force is given by $\mathbf{F}_{Lorentz} = \mathbf{J} \times \mathbf{B}$ where \mathbf{J} is the current density. It may be noted that the magnetic field in the above is the total field, i.e. the sum of the applied and induced fields. The effect of the Lorentz force on the hydrodynamics can be incorporated through \mathbf{F}_{ext} term appearing in Eqs. (1) or (15). The total magnetic field \mathbf{B} evolves with time due to its interaction with the flow field and diffusion, which is generally represented by the magnetic induction equation [58]. In LBM, this magnetic induction equation is simulated by a solving a kinetic equation for the vector distribution function \mathbf{g}_α which is given by [50, 51]

$$\mathbf{g}_\alpha(\mathbf{x} + \Xi_\alpha \delta_t, t + \delta_t) - \mathbf{g}_\alpha(\mathbf{x}, t) = -\frac{1}{\tau_m} (\mathbf{g}_\alpha - \mathbf{g}_\alpha^{eq}), \quad (39)$$

where Ξ_α represents the free-streaming velocity directions for the magnetic vector distribution function. The magnetic relaxation time parameter τ_m is related to the magnetic resistivity η by $\eta = \theta_m \left(\tau_m - \frac{1}{2} \right) \delta_t$ where $\theta_m = c^2/3$ and $\theta_m = c^2/4$ in 2D and 3D, respectively. The equilibrium distribution function \mathbf{g}_α^{eq} is a function of both velocity and magnetic fields $\mathbf{g}_\alpha^{eq} = \mathbf{g}_\alpha^{eq}(\mathbf{u}, \mathbf{B})$ [50, 51]. The magnetic field and current density can be obtained by taking appropriate moments of the vector distribution function [50]

$$\mathbf{B} = \sum_{\alpha=0}^{b_m} \mathbf{g}_\alpha, \quad (40)$$

$$(\mathbf{J})_k = -\frac{1}{\mu_m} \frac{1}{\theta_m \tau_m} \epsilon_{ijk} \sum_{\alpha=0}^{b_m} g_{\alpha i} \Xi_{\alpha j}, \quad (41)$$

where ϵ_{ijk} is the Levi-Civita permutation tensor, μ_m is the magnetic permeability and b_m is the number of free-streaming directions for the magnetic vector distribution function.

RESULTS AND DISCUSSION

First, some examples of the application of the MRT LBM are discussed in this section. As shown and discussed in [34-37], for standard multiphase flow problems such as 2D capillary waves and 3D drop oscillations it is found that an order of magnitude reduction in viscosities is possible with the application of the MRT model in lieu of the BGK model. We first consider the breakup of a cylindrical liquid column through Rayleigh instability resulting in the formation of drops, a fascinating problem of long standing theoretical and practical interests. In a seminal work, Rayleigh (1878) [59] showed through a linear stability analysis of an inviscid column of cylindrical liquid of radius R_c that the column will be unstable if the axisymmetric wavelength λ_d of any disturbance is longer than its circumference, i.e. the wave number $k^* = 2\pi R_c / \lambda_d$ is less than one. Later, the theoretical analysis was extended to more realistic conditions by including viscosity. In the last three decades, several experimental and numerical investigations have also been performed. To evaluate the LBM model, the Rayleigh capillary instability for different wavenumbers was studied [29]. Initial studies carried out with $k^* > 1$ showed that the liquid does not break-up.

We will now present results of a case with break-up. All the results discussed in the section will be in *lattice units* unless otherwise stated. That is, the velocities are scaled by the particle velocity c and the distances by the lattice spacing δ_x . Consider a cylindrical liquid column of radius $R_c = 45$ subject to an axisymmetric sinusoidal wavelength $\lambda_d = 600$, i.e. $k^* = 0.47$. To simulate the dynamics of instability for this wavenumber, we consider a domain discretized by 601×151 lattice nodes with fluids having densities $\rho_G = 0.1$, $\rho_L = 0.4$, and viscosities $\nu_G = \nu_l = 6.667 \times 10^{-2}$ and surface tension parameter $\kappa = 0.10$. Since $k^* < 1$, it is expected that the liquid column would eventually break up. Figure 2 shows the configurations of the liquid column at different times. The disturbance grows with time. The column breaks up, forming a satellite droplet. The drop size distribution, i.e. the non-dimensional size of main and satellite drops, as a function of wave number, k^* was quantitatively studied in [29]. The results were compared with the solution based on the third-

order perturbation analysis of the Navier-Stokes equations (NSE) [60], experimental data [61] and boundary integral [62] and finite element [63] solutions of the NSE. The LBM model was found to be able to reproduce the drop size distribution quantitatively within 12%.

The next example of the MRT LBM is the simulation of binary drop collisions, which was studied for a range of parameters in [38]. At low Weber numbers, i.e. $We = 20$, the colliding drops coalesce permanently with the formation of stable microbubble, which was observed in experiments [64] and in prior simulations based on level set method [65]. At higher We , eventual separation of colliding drops are expected [66]. Figure 3 shows the temporal evolution of interfaces of equal-size colliding drops for a Weber number of 100 with a Reynolds number of 384.5, Ohnesorge number of 0.589 and density ratio, r of 4, and dynamic viscosity ratio, λ of 4. T in the figure is a non-dimensional time defined as $tU/(R_1 + R_2)$ where t is time, U is relative velocity and R_1 and R_2 are radii of drops. The collision dynamics exhibit the different phases of deformation and internal flow as pointed in [67]. Upon initial deformation of the temporarily coalesced drop, shown at $T = 0.601$, it undergoes radial stretching shown at times $T = 1.551$. The rim recedes at $T = 6.297$. It then undergoes axial stretching (see $T = 9.461$ and $T = 19.904$). Such stretching results subsequently in bulbous ends which breakup through the well-known 'end-pinching' mechanism observed experimentally and computationally when drops are subjected to axial stretching [68, 69].

We will now discuss an application of the regularized LBM. In the case of single-phase flows, it was shown that the regularized LBM can achieve lowering of viscosities by a factor of about 7 as compared to the standard BGK model [41]. Initial computations of the formation of static drops with the regularized model for multiphase flows [42] results in a reduction in the viscosity by a factor of at least 2 as compared to the standard model. Here, we discuss the simulation of the Rayleigh-Taylor instability using the regularized model. We consider a single-mode perturbation of the interface between the heavier fluid at the top and the lighter fluid at the bottom, with densities, $\rho_L = 0.6$, $\rho_G = 0.1$ respectively, and subjected to gravity. The domain is discretized by 128×512 lattice grids where the first quantity represents the width W . Gravity g is applied by setting the velocity scale $u^{RT} = \sqrt{Wg}$ to be equal to 0.04 so that the flow is in the weakly compressible range. The relaxation parameter is chosen such that the Reynolds number $Re = 128$. For the chosen densities, the Atwood number $A = (\rho_L - \rho_G)/(\rho_L + \rho_G)$ becomes 0.714. Surface

tension is not considered for simplicity. Figure 4 shows the interface evolution at different times T which is a non-dimensional time expressed by $T = tu^{RT}/W$. Notice that the heavier fluid flows down as a spike while the lighter fluid rises to form bubbles. At later times, the heavier fluid starts to roll up into two counter-rotating vortices. These are standard features of Rayleigh-Taylor instability [20, 70, 71], which the regularized LBM appear to reproduce well.

Next, we discuss some preliminary computations carried out using the time-splitting LBM. Figure 5 shows the planar interfaces at two different times represented by zero level sets which separate a heavier fluid at the bottom and a lighter fluid at the top. The domain is discretized by 50×50 grids, in which the interface is set initially midway. In this simulation, the density ratio is 12. The relaxation parameters τ for both the phases are equal to 0.99 each. The surface tension coefficient σ is kept equal to 0.0728 but since the interface is flat, and does not undergo deformation, curvature effects are small. The level set formulation is used to capture the interface. In this regard, a 3rd order Runge-Kutta total variation diminishing (TVD) scheme for time integration and a 5th order weighted essentially non-oscillatory (WENO) scheme for spatial derivatives is employed [72]. It is found that the time-splitting approach is able to maintain stable interface at longer times. To test whether the approach is able to maintain stable curved interfaces, a bubble is kept in a medium such that the density ratio is 2 and subjected to external acceleration. Figure 6 shows the deformation of a moving bubble at different times and the computation remains stable at longer times. While these initial computations are encouraging, more detailed evaluations of the time-splitting approach are in progress.

We will now present some applications of the MHD multiphase flows computed using the LBM. First, we consider an electrically conducting drop subjected to an initial velocity in the presence a spatially varying imposed field that is normal to the velocity. A drop of radius $R_d = 24$ is initially placed in a domain discretized by $L_x \times L_y = 300 \times 300$ lattice grids, where x represents the direction of the drop's initial velocity. The applied magnetic field is given by $B_y(x) = B_0/(1 + \exp(-x'/x_0))$, where $x' = x - L_x/2$ and B_0 determines the magnitude of the field and x_0 controls the sharpness of the spatial variation. We consider $B_0 = 0.002$, $x_0 = 0.15(L_y/2)$ and the initial velocity $u_0 = 0.015$. The set of physical parameters employed are the following: densities $\rho_G = 0.1$, $\rho_L = 0.6$, surface tension parameter $\kappa = 0.03$, relaxation parameters

that determine fluid viscosities $\tau_G = 0.54, \tau_L = 0.54$, and those that control magnetic diffusivities $\tau_{mG} = 0.55, \tau_{mL} = 0.55$ and magnetic permeability $\mu_m = 1$.

Figure 7 shows the drop configurations and the normal component of the total magnetic field, i.e. imposed and the induced fields, at different times. The initial magnetic field has spatial variation around the center of the domain, with the minimum and the maximum on the left and right sides, respectively, with respect to the center. As the drop moves forward, it is opposed by the viscous drag and the Lorentz force arising due to the interaction between the velocity and magnetic fields. In the initial stages, prior to the drop reaching the center of the domain, the opposing force is predominantly due to viscous effects. This results in the expected deformation of the drop into oval shape ($t = 5000$), which then relaxes towards its original shape due to surface tension effects. However, as the drop approaches the region of spatial variation in the magnetic field ($t = 9000$), it encounters increasingly greater electromagnetic drag. Since the magnetic diffusion relaxation time scales are comparable to that of the viscous scales, the motion of drop modifies the total magnetic field, with the maximum field strength just in front of the drop. As the drop moves further from the center, it is considerably decelerated by the increasing electromagnetic drag.

Another MHD example considered involves the simulation of an electrically conducting liquid film flow in an inclined channel driven by pressure gradient and gravity and subjected to a spatially varying imposed field. The domain size is $L_x \times L_y = 300 \times 60$ and the form of the imposed magnetic field variation including B_0 and x_0 are the same as in the previous case. The physical parameters are also the same as in the previous case expect the following: $\tau_G = \tau_L = 0.70$ $\tau_{mG} = \tau_{mL} = 0.55$. The imposed pressure gradient $dp/dx = -5 \times 10^{-7}$. Figure 8 shows the configurations of the liquid film at different times. The interactions between the pressure gradient, gravity and the spatially varying magnetic field results in surface wave motion. Figure 9 shows the velocity profiles at three different cross-sections when $t = 30000$. The velocity profile in the cross-section that is under the influence of magnetic field ($x = 225$) shows the expected flattening due to the opposing Lorentz force effects.

SUMMARY AND OUTLOOK

In this paper, we reviewed some recent developments of the lattice Boltzmann method (LBM) for applications to interfacial multiphase fluid mechanics problems. The method is based on physical concepts that can be traced to kinetic theory. While it has attracted considerable attention in recent years, the method faces certain computational limitations when applied to problems of practical interest. This paper has focused on the discussion of two such limitations. First, the standard LBM becomes unstable at lower shear viscosities, or equivalently, higher Reynolds numbers. Two approaches have been discussed to alleviate this limitation. One is the introduction of the multiple-relaxation time (MRT) models that allows independent control of various relaxation time scales. By appropriately adjusting these time scales, stability at viscosities which can be about an order of magnitude smaller as compared to that with the standard models can be achieved. As examples, the application of the MRT models to simulations of Rayleigh breakup of cylindrical liquid columns and drop collisions show good agreement with prior data [29, 38].

The second approach is based on regularizing/renormalizing the pre-collision distribution functions while retaining the single-relaxation time model. This leads to a simpler approach for improving stability. Greater stability is achieved by eliminating the unwanted kinetic modes inherent in the standard BGK model. Initial studies have shown that it is able to achieve lowering of viscosities by a factor of atleast two as compared to the standard BGK model without regularization. Simulation of Rayleigh-Taylor instability using the regularized model shows features that are consistent with the prior simulations.

Second, the standard LBM becomes unstable when there is a large mismatch in density of the fluids. While a solution to this problem based on kinetic theory is not yet forthcoming, some efforts have been made to address this issue from a computational point of view. In this paper, we have proposed a time-splitting approach to alleviate the density ratio problem. In this approach, fluid motions in each phase are solved separately by means of the LBM, interfacial motion is advected by means level sets and the interfacial boundary conditions are matched sequentially by a procedure based on the Chapman-Enskog analysis. In contrast to the other approaches which treat the interface as diffuse, this technique maintains a sharp interface. While analogous to the ghost-fluid method, it does not involve the solution of the Poisson-type pressure equation. This maintains the local nature of the LBM formulation and its easy parallelizability. Preliminary calculations using this approach are encouraging.

Computations of MHD multiphase flows using LBM, for the first time, are reported in this paper. First, we observe

through simulations that an electrically conducting drop subjected to an initial velocity and passing through a sharply varying magnetic field in space encounters a significant electromagnetic drag thereby decelerating it. Second, it is seen that electrically conducting liquid film flow past an inclined wall driven by a pressure gradient and gravity and in the presence of sharply varying magnetic field in space results in significant surface wave motion.

While the recent developments of the LBM have been significant, much remains to be done. Highlighting just a few possible future directions, techniques that introduce *adaptive* refinements of lattice grids in LBM for multiphase flows appear to be lacking. While the development of axisymmetric LBM [29] is a first step in achieving high fidelity simulations, adaptive mesh refinement is required in general cases. The approach discussed in [73] may be extended in a similar vein as in [74] with adaptive capabilities for multiphase flow applications. Almost all the work on LBM for multiphase flows has been restricted to isothermal applications. This is because when energy transport is considered within the LBM framework, it is prone to numerical instabilities. Recently, successful applications have been attained by employing a hybrid approach, in which the fluid dynamics is represented by the LBM and the energy transport by a conventional approach such as the finite-difference method, which has the same stencil as the lattice, with an appropriate coupling between the two approaches [75]. Extension of this idea to LBM multiphase flow models would open up many new applications.

ACKNOWLEDGEMENTS

The multiple relaxation time (MRT) LBM work was done under the supervision of Professor John Abraham at Purdue University during the period 2002-2004 by the first author of this paper and Dr. Michael E. McCracken now at ExxonMobil Corporation. Interactions with these individuals are gratefully acknowledged. We acknowledge support by the U.S. Department of Energy under Grant No. DE-FG02-03ER83715.

REFERENCES

1. Tryggvason, G., Bunner, B., Esmaeeli, A., Juric, D., Al-Rawahi, N., Tauber, W., Han, J., Nas, S., and Jan. Y.-J., 2001, "A Front Tracking Method for Computations of Multiphase Flow", *Journal of Computational Physics*, **169**, 708-759.
2. Scardovelli, R. and Zaleski, S., 1999, "Direct Numerical Simulation of Free-Surface and Interfacial Flow", *Annual Review of Fluid Mechanics*, **31**, 567-603.
3. Sethian, J.A. and Smereka, P., 2003, "Level Set Methods for Fluid Interfaces", *Annual Review of Fluid Mechanics*, **35**, 341-372.
4. Badalassi, V., Cenicerros, H. and Banerjee, S., 2003, "Computation of Multiphase Systems with Phase Field Models", *Journal of Computational Physics*, **190**, 371-397.
5. Chorin, A.J., 1968, "Numerical Solution of the Navier-Stokes Equations", *Mathematics of Computation*, **23**, 341-353.
6. Bell, J.B., Colella, P., and Glaz, H.M., 1989, "A Second-Order Projection Method for the Incompressible Navier-Stokes Equations", *Journal of Computational Physics*, **85**, 257-283.
7. Chen, S. and Doolen, G., 1998 "Lattice Boltzmann Method for Fluid Flows", *Annual Review of Fluid Mechanics*, **30**, 329-364.
8. Succi, S., 2001, *The Lattice Boltzmann Equation for Fluid Dynamics and Beyond*. Oxford University Press, New York.
9. He, X. and Luo, L.-S., 1997, "Theory of the Lattice Boltzmann Method: From the Boltzmann Equation to the Lattice Boltzmann Equation", *Physical Review E*, **56**, 6811-6817.
10. Benzi, R., Succi, S., and Vergassola, M., 1992, "The Lattice Boltzmann Equation: Theory and Applications", *Physics Reports*, **3**, 147-197.
11. Qian, Y., Succi, S., and Orszag, S.A., 1995, "Recent Advances in Lattice Boltzmann Computing", *Annual Review of Computational Physics*, **3**, 195-242.
12. Succi, S., Karlin, I., and Chen, H., 2002, "Role of H Theorem in Lattice Boltzmann Hydrodynamic Simulations", *Reviews of Modern Physics*, **74**, 1203-1220.
13. Nourgaliev, R., Dinh, T., Theofanous, T., and Joseph, D., 2003, "The Lattice Boltzmann Method: Theoretical Interpretation, Numerics and Implications". *International Journal of Multiphase Flow*, **23**, 117-169.
14. Yu, D., Mei, R., Luo, L.-S., and Shyy, W., 2003, "Viscous Flow Computations with the Method of Lattice Boltzmann Equation", *Progress in Aerospace Sciences*, **39**, 99-120.
15. Wolf-Gladrow, D., 2000, *Lattice-Gas Cellular Automata and Lattice Boltzmann Models, Lecture Notes in Mathematics*, No. 1725. Springer, Berlin.
16. Gunstensen, A., Rothman, D., Zaleski, S., and Zanetti, G., 1991, "Lattice Boltzmann Model for Immiscible Fluids", *Physical Review A*, **43**, 4320-4327.
17. Grunau, D., Chen, S., and Eggert, K., 1993, "A Lattice Boltzmann Model for Multiphase Fluid Flows", *Physics of Fluids A*, **5**, 2557-2562.
18. Shan, X. and Chen, H., 1993, "Lattice Boltzmann Model of Simulating Flows with Multiple Phases and Components", *Physical Review E*, **47**, 1815-1819.
19. He, X., Shan, X., and Doolen, G., 1998, "Discrete Boltzmann Equation Model for Nonideal Gases", *Physical Review E*, **57**, R13-R16.
20. He, X., Chen, S., and Zhang, R., 1999, "A Lattice Boltzmann Scheme for Incompressible Multiphase Flow

- and its Application in Simulation of Rayleigh-Taylor Instability”, *Journal of Computational Physics*, **152**, 642-663.
21. Swift, M., Orlandini, S., Osborn, W., and Yeomans, J. 1996, “Lattice Boltzmann Simulations of Liquid-Gas Binary-fluid Systems”, *Physical Review E*, **54**, 5041-5042.
 22. Swift, M., Osborn, W., and Yeomans, J., 1995, “Lattice Boltzmann Simulations of Nonideal Fluids”, *Physical Review Letters*, **75**, 830-833.
 23. Luo, L.-S., 2000, “Theory of the lattice Boltzmann method: Lattice Boltzmann Models for Nonideal gases”, *Physical Review E*, **62**, 4982-4996.
 24. Inamuro, T., Konishi, N., and Ogino, F., 2000, “A Galilean invariant model of the lattice Boltzmann method for multiphase fluid flows using free-energy approach”, *Computer Physics Communications*, **129**, 32-45.
 25. He, X., Zhang, R., Chen, S., and Doolen, G.D., 1999, “On Three Dimensional Rayleigh-Taylor Instability”, *Physics of Fluids*, **11**, 1143-1152.
 26. Sankaranarayanan, K., Kevrekidis, I.G., Sundaresan, S., Lu, J., and Tryggvason, G., 2003, “A Comparative Study of Lattice Boltzmann and Front – Tracking Finite-Difference Methods for Bubble Simulations”, *International Journal of Multiphase Flows*, **29**, 109-116.
 27. Inamuro, T., Tomita and R., Ogino, F., 2003, “Lattice Boltzmann Simulations of Drop Deformation and Breakup in Shear Flows”, *International Journal of Modern Physics B*, **17**, 21-26.
 28. Premnath, K. N. and Abraham, J., 2005, “Lattice Boltzmann Simulations of Drop-Drop Interactions in Two-Phase Flows”, *International Journal of Modern Physics C*, **16**, 25-45.
 29. Premnath, K. N. and Abraham, J., 2005, “Lattice Boltzmann Model for Axisymmetric Multiphase Flows”, *Physical Review E*, **71**, 056706:1-14.
 30. Bhatnagar, P., Gross, E., and Krook, M., 1954, “A Model for Collision Processes in Gases. I. Small Amplitude Processes in Charged and Neutral One-Component Systems”, *Physical Review*, **94**, 511-525.
 31. d’Humières, D., 1992, “Generalized Lattice Boltzmann Equations”, In *Rarefied Gas Dynamics: Theory and Simulations*, *Progress in Aeronautics and Astronautics*, **159**, 450-458.
 32. Lallemand, P. and Luo, L.-S., 2000, “Theory of the Lattice Boltzmann Method: Dispersion, Isotropy, Galilean Invariance, and Stability”, *Physical Review E*, **61**, 6546-6562.
 33. d’Humières, D., Ginzburg, I., Krafczyk, M., Lallemand, P., and Luo, L.-S., 2002, “Multiple-Relaxation-time Lattice Boltzmann Models in Three-dimensions”, *Philosophical Transactions of the Royal Society of London, Series A*, **360**, 437-351.
 34. McCracken, M. E. and Abraham, J., 2005, “Multiple Relaxation Time Lattice Boltzmann Model for Multiphase Flow”, *Physical Review E*, **71**, 036701:1-9.
 35. McCracken, M. E., 2004, “Development and Evaluation of Lattice Boltzmann Models for Investigations of Liquid Break-Up”, *Ph.D. Thesis*, Purdue University, West Lafayette, IN.
 36. Premnath, K. N. and Abraham, J., 2005, “Three-Dimensional Multi-Relaxation Time (MRT) Lattice Boltzmann Models for Multiphase Flows”, *Journal of Computational Physics*, submitted.
 37. Premnath, K. N., 2004, “Lattice Boltzmann Models for Simulations of Drop-Drop Collisions”, *Ph.D. Thesis*, Purdue University, West Lafayette, IN.
 38. Premnath, K. N. and Abraham, J., 2005, “Simulations of Binary Drop Collisions with a Multiple Relaxation Time Lattice Boltzmann Method”, *Physics of Fluids*, submitted.
 39. McCracken, M. E. and Abraham, J., 2005, “Simulations of Liquid Break-Up with a Axisymmetric, Multiple Relaxation Time, Index Function Lattice Boltzmann Model”, *International Journal of Modern Physics C*, to appear.
 40. Premnath, K. N., McCracken, M.E. and Abraham, J., 2005, “A Review of Lattice Boltzmann Methods for Multiphase Flows Relevant to Engine Sprays”, *Society of Automotive Engineers 2005 World Congress*, Detroit, MI.
 41. Latt, J. and Chopard, B., 2005, “Lattice Boltzmann Method with Regularized Non-Equilibrium Distribution Functions”, *Phys. Rev. Lett.* Submitted (See also arXiv:physics/0506157).
 42. Premnath, K.N., 2005, “Regularized Lattice Boltzmann Model with Force Fields and its Applications to Multiphase Flows”, unpublished notes.
 43. Teng, S.L., Chen, Y., and Ohashi, H., 2000, “Lattice Boltzmann Simulation of Multiphase Fluid Flows Through Total Variation Diminishing with Artificial Compression Scheme”, *International Journal of Heat and Fluid Flow*, **21**, 112-121.
 44. Inamuro, T., Ogata, T., Tajima, S., and Konishi, N. 2004, “A Lattice Boltzmann Method for Incompressible Two-phase Flows with Large Density Differences”, *Journal of Computational Physics*, **198**, 628-644.
 45. Lee, T. and Lin, C.-L., 2005, “A Stable Discretization of the Lattice Boltzmann Equation for Simulation of Incompressible Two-Phase Flows at High Density Ratio”, *Journal of Computational Physics*, **206**, 16-47.
 46. Premnath, K.N., 2005, “Lattice Boltzmann Interfacial Fields Reconstruction Procedure Through Time-Splitting for Multiphase Flows Subjected to External Force Fields”, unpublished notes.
 47. Fedkiw, R., Aslam, T., Merriman, B., and Osher, S., 1999, “A Non-oscillatory Eulerian Approach to Interfaces in Multimaterial Flows (The Ghost Fluid Method)”, *Journal of Computational Physics*, **152**, 457-492.

48. Kang, M., Fedkiw, R., and Liu, X.-D., 2000, "A Boundary Condition Capturing Method for Multiphase Incompressible Flow", *Journal of Scientific Computing*, **15**, 323-359.
49. Adbou, M., Ying, A., Morley, N., *et al.*, 2001, "On the exploration of innovative concepts for fusion chamber technology – APEX Interim Report Overview", *Fusion Engineering and Design*, **54**, 181-247.
50. Dellar, P.J., 2002, "Lattice Kinetic Schemes for Magnetohydrodynamics", *Journal of Computational Physics*, **179**, 95-126.
51. Breyiannis, G. and Valougeorgis, D., 2004, "Lattice Kinetic Simulations in Three-Dimensional Magnetohydrodynamics", *Physical Review E*, **65**, 065702 (R): 1-4.
52. Rowlinson, J. and Widom, B., 1982. *Molecular Theory of Capillarity*. Clarendon Press, Oxford.
53. Chapman, S. and Cowling, T., 1964, *Mathematical Theory of Non-Uniform Gases*. Cambridge University Press, London.
54. Carnahan, N. and Starling, K., 1969, "Equation of State for Nonattracting Rigid Spheres", *Journal of Chemical Physics*, **51**, 635-636.
55. Evans, R., 1979, "The Nature of the Liquid-Vapor Interface and other Topics in the Statistical Mechanics of Non-Uniform, Classical Fluids", *Advances in Physics*, **28**, 143.
56. Ginzburg, I. and d'Humieres, D., 1996, "Local Second-Order Boundary Methods for Lattice Boltzmann Models", *Journal of Statistical Physics*, **84**, 927-971.
57. Ginzburg, I. and Steiner, K., 2003, "Lattice Boltzmann Model for Free Surface Flow and its Application to Filling Process in Casting", *Journal of Computational Physics*, **185**, 61-99.
58. Muller, U., and Buhler, L., 2001. *Magnetohydrodynamics in Channels and Containers*, Springer, New York.
59. Rayleigh, L. 1878, "On the Instability of Jets", *Proceedings of the London Mathematical Society*, **10**, 4-13.
60. Lafrance, P. 1975, "Nonlinear Breakup of a Laminar Liquid Jet", *Physics of Fluids*, **18**, 428-432.
61. Rutland, D. and Jameson, G. 1971, "A Non-Linear Effect in the Capillary Instability of Liquid Jets", *Journal of Fluid Mechanics*, **46**, 267-271.
62. Mansour, N. and Lundgren, T.S., 1990, "Satellite Formation in Capillary Jet Breakup", *Physics of Fluids*, **2**, 1141-1144.
63. Ashgriz, N. and Mashayek, F., 1995, "Temporal Analysis of Capillary Jet Breakup", *Journal of Fluid Mechanics*, **291**, 163-190.
64. Ashgriz, N. and Poo, Y., 1990, "Coalescence and Separation in Binary Collisions of Liquid Drops", *Journal of Fluid Mechanics*, **221**, 183-204.
65. Pan, Y. and Suga, K., 2004, "Numerical Simulation of Liquid Droplet Binary Collision", *In Proceedings of the Fifth International Conference on Multiphase Flows*, Yokohama, Japan.
66. Qian, J. and Law, C., 1997, "Regimes of Coalescence and Separation in Droplet Collision", *Journal of Fluid Mechanics*, **331**, 59-80.
67. Roisman, I., 2004, "Dynamics of Inertia Dominated Binary Drop Collisions", *Physics of Fluids*, **16**, 3438-3449.
68. Stone, H., Bentley, B., and Gary Leal, L., 1986, "An Experimental Study of Transient Effects in the Breakup of Viscous Drops", *Journal of Fluid Mechanics*, **173**, 131-158.
69. Stone, H. and Gary Leal, L., 1989, "Relaxation and Breakup of an Initially Extended Drop in an Otherwise Quiescent Fluid", *Journal of Fluid Mechanics*, **198**, 399-427.
70. Daly, B.J., 1967, "Numerical Study of Two Fluid Rayleigh-Taylor Instabilities", *Physics of Fluids*, **10**, 297-307.
71. Tryggvason, G., 1988, "Numerical Simulation of the Rayleigh-Taylor Instability", *Journal of Computational Physics*, **75**, 253-282.
72. Nave, J.-C., 2004, "Direct Numerical Simulation of Liquid Films", Ph.D. thesis, University of California Santa Barbara.
73. Filippova, O. and Hanel, D., 1998, "Grid Refinement for Lattice-BGK Models", *Journal of Computational Physics*, **147**, 219-228.
74. Sussman, M., Almgren, A.S., Bell, J.B., Colella, P., Howell, L.H. and Welcome, M.L., 1999, "An Adaptive Level Set Approach for Incompressible Two-Phase Flows", *Journal of Computational Physics*, **148**, 81-124.
75. Lallemand, P. and Luo, L.-S., 2003, "Theory of the Lattice Boltzmann Method: Acoustic and Thermal Properties in Two and Three Dimensions", *Physical Review E*, **68**, 036706: 1-25.

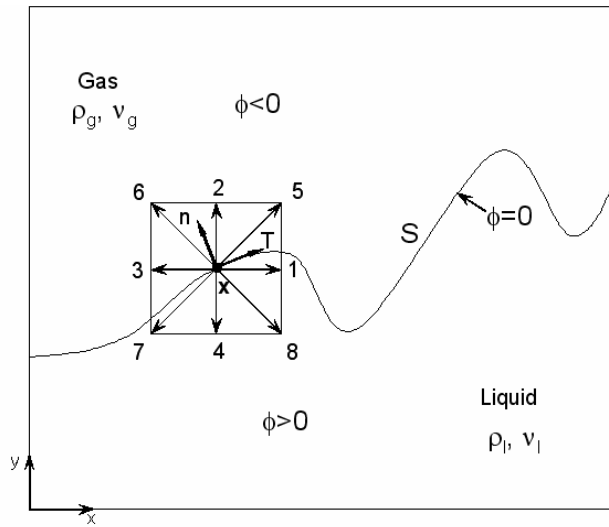


Figure 1. SCHEMATIC VIEW OF LOCAL COORDINATE SYSTEM $\{n, T\}$ ON THE INTERFACE S BETWEEN LIQUID AND GAS PHASES. DOMAIN IS DISCRETIZED BY MEANS OF LATTICE NODES.

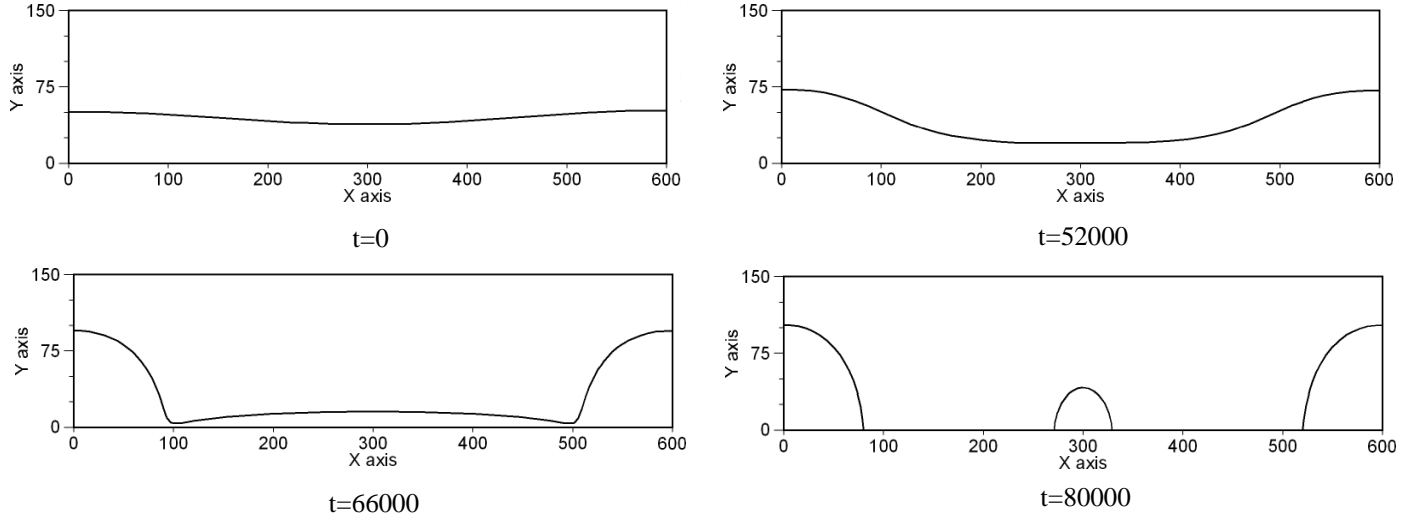


Figure 2. CONFIGURATIONS OF A CYLINDRICAL LIQUID COLUMN AT DIFFERENT TIMES UNDERGOING RAYLEIGH BREAKUP AND GENERATION OF SATELLITE DROPLET [29]; $k^* = 0.47$, $\rho_G = 1$, $\rho_L = 0.4$, $v_L = v_G = 6.667 \times 10^{-2}$.

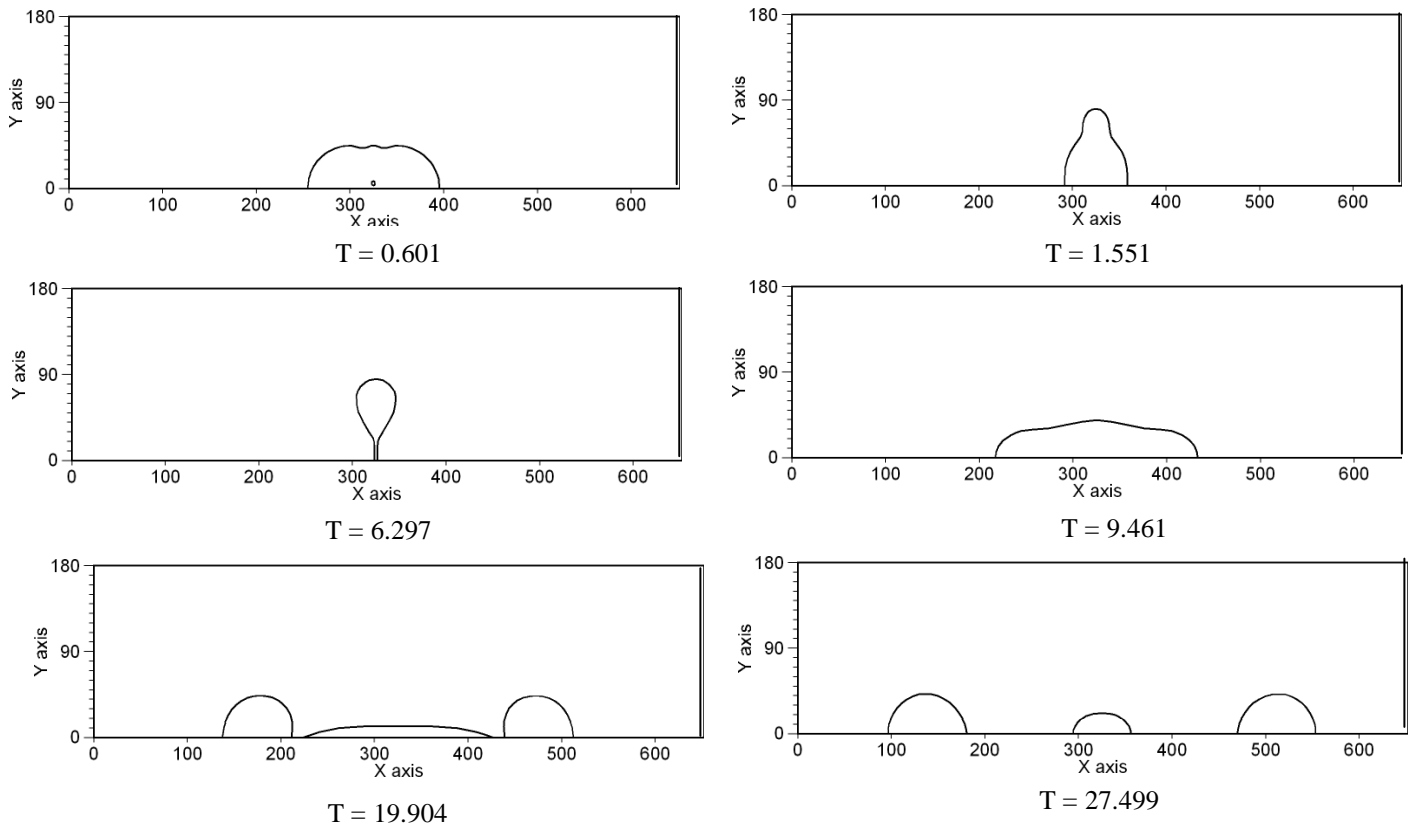


Figure 3. COLLIDING DROPS AT DIFFERENT TIMES, T SIMULATED USING MRT LBM [38];
 $We = 100$, $Re = 384.5$, $Oh = 0.589$, $r = 4$, $\lambda = 4$.

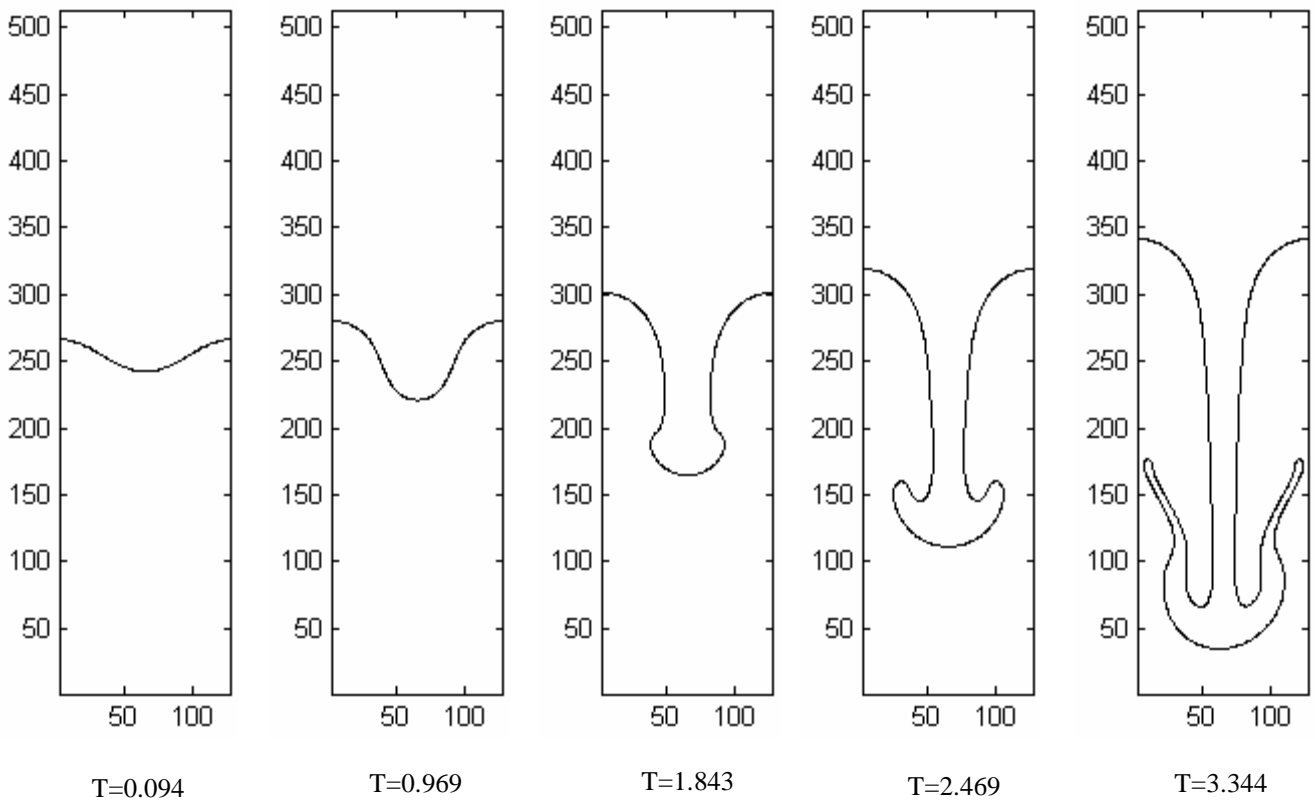
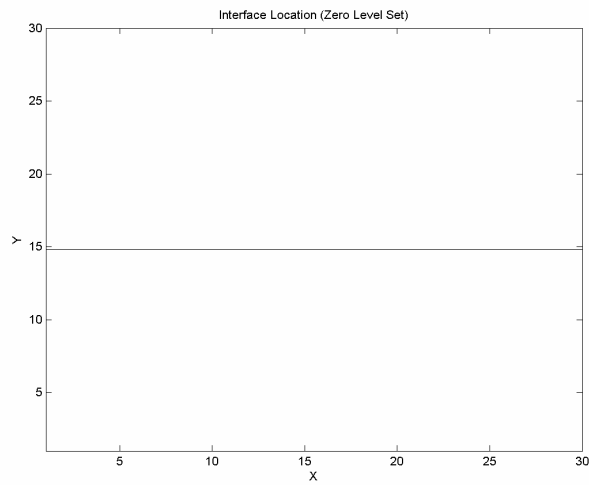
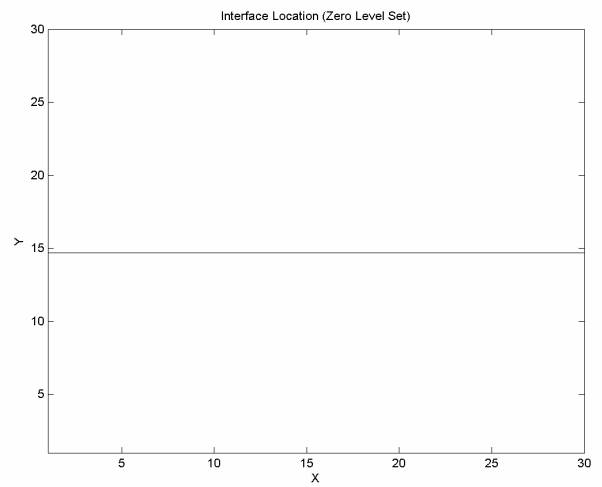


Figure 4. INTERFACE EVOLUTION FROM A SINGLE-MODE PERTURBATION UNDERGOING RAYLEIGH-TAYLOR INSTABILITY SIMULATED USING REGULARIZED LBM; $Re = 128$, $A = 0.714$.

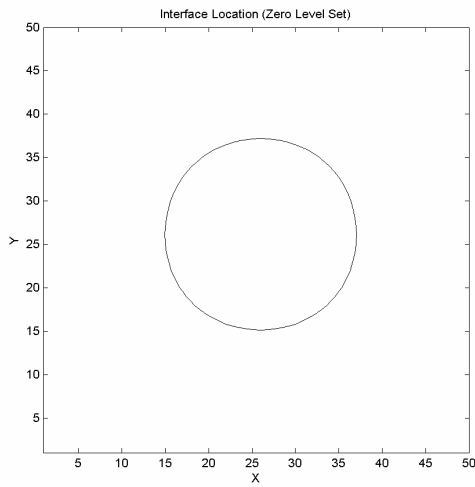


t=10

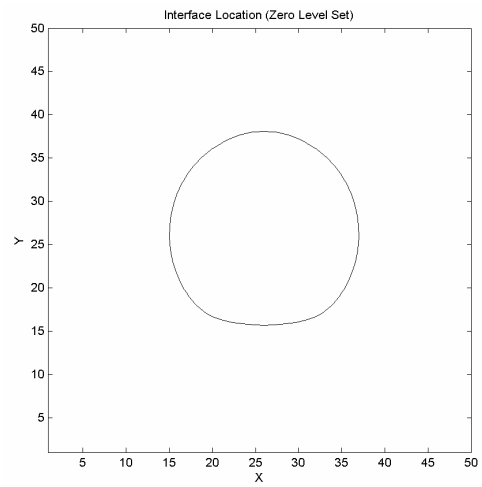


t=1000

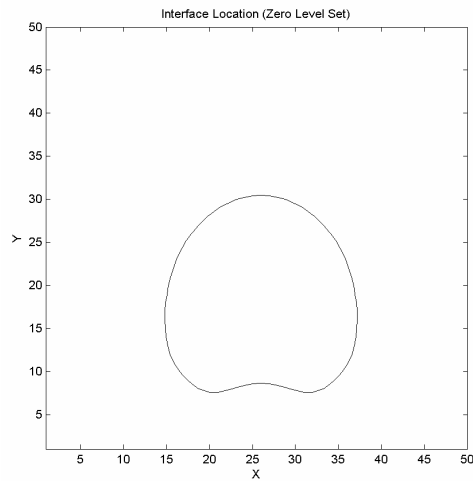
Figure 5. STABLE PLANAR INTERFACE SIMULATED USING THE TIME-SPLITTING LBM.



t=100



t=2400



t=5200

Figure 6 DEFORMATION OF A RISING BUBBLE IN THE PRESENCE OF GRAVITY SIMULATED USING THE TIME-SPLITTING LBM.

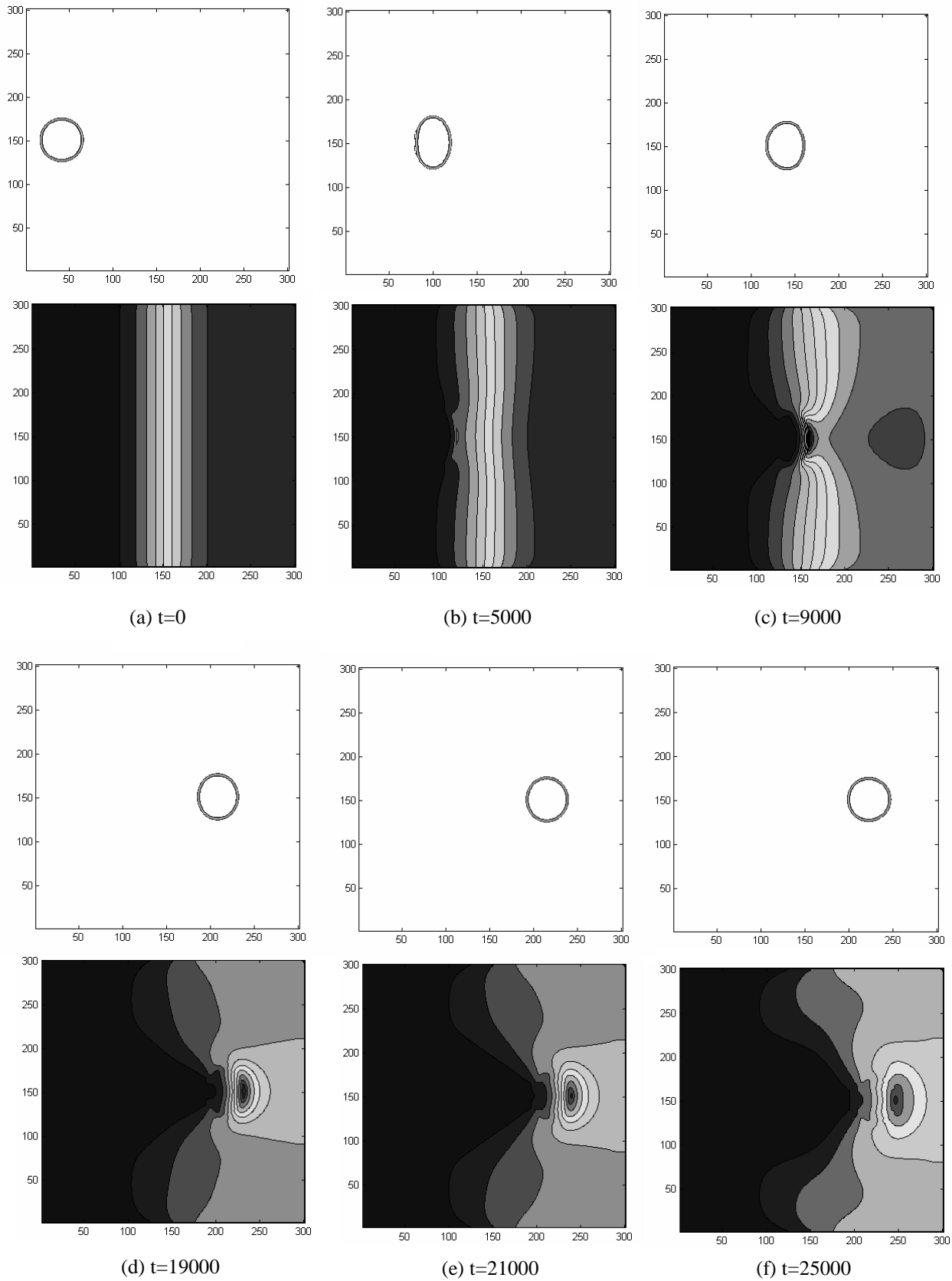


Figure 7. DROP CONFIGURATIONS AND NORMAL COMPONENT OF MAGNETIC FIELD AT DIFFERENT TIMES; $\kappa=0.03$, $\rho_G=0.1$, $\rho_L=0.6$, $\tau_L=\tau_G=0.54$, $\tau_{mL}=\tau_{mG}=0.55$, $\mu_m=1$.

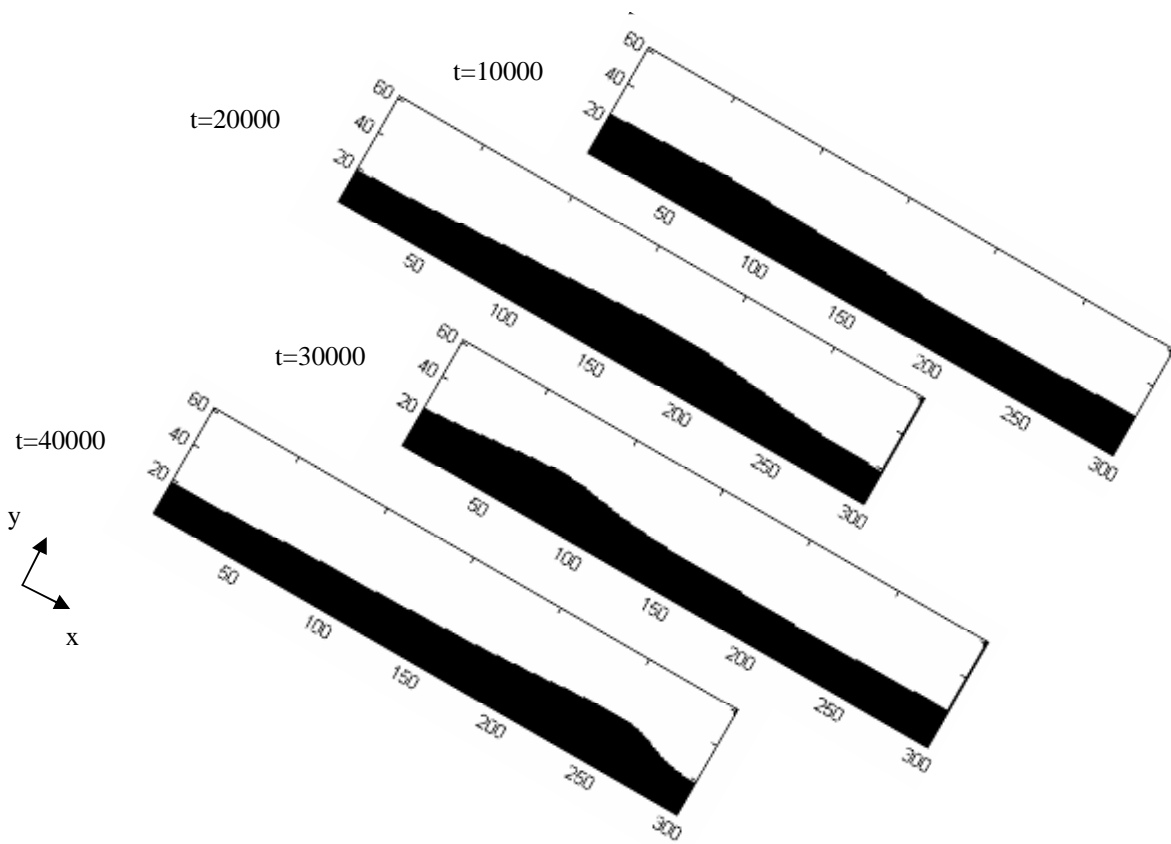


Figure 8. CONFIGURATIONS OF LIQUID FILM DRIVEN BY PRESSURE GRADIENT AND GRAVITY SUBJECTED TO A SPATIALLY VARYING MAGNETIC FIELD; $\kappa=0.03$, $\rho_G=0.1$, $\rho_L=0.6$, $\tau_L=\tau_G=0.70$, $\tau_{mL}=\tau_{mG}=0.70$, $\mu_m=1$.

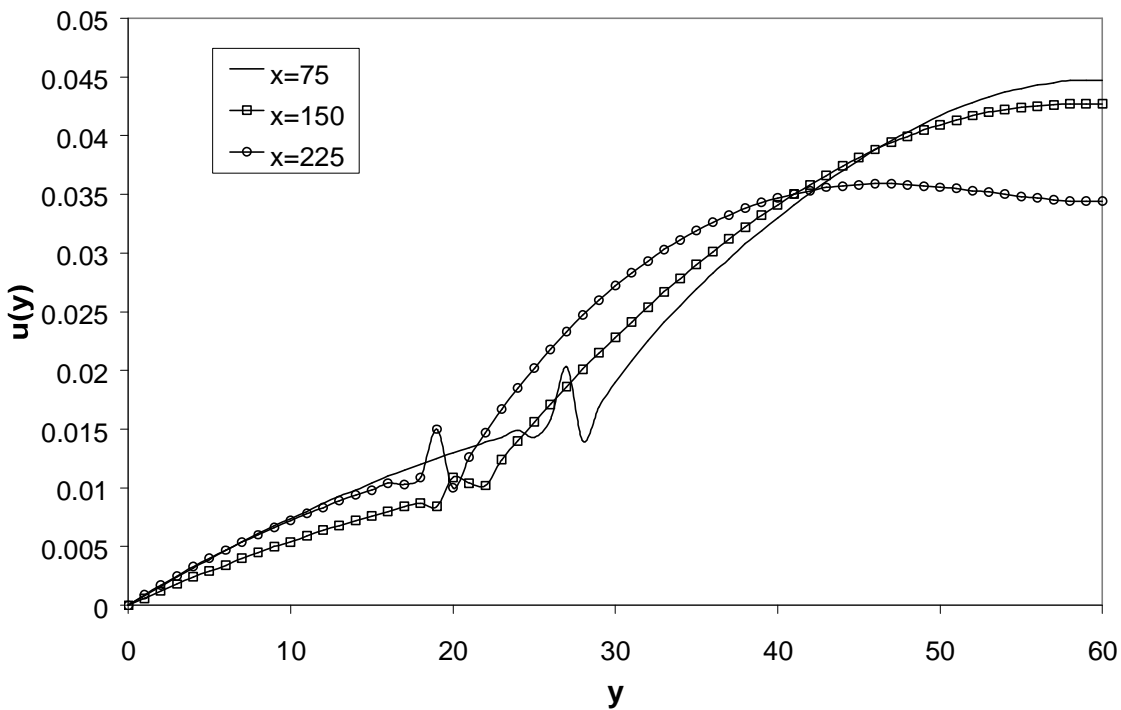


Figure 9. VELOCITY PROFILES AT DIFFERENT CROSS SECTIONS OF THE FILM FLOW DRIVEN BY PRESSURE GRADIENT AND GRAVITY SUBJECTED TO A SPATIALLY VARYING MAGNETIC FIELD; $\kappa=0.03$, $\rho_G=0.1$, $\rho_L=0.6$, $\tau_L=\tau_G=0.70$, $\tau_{mL}=\tau_{mG}=0.70$, $\mu_m=1$.